Asociación Argentina
de Mecánica Computacional

Mecánica Computacional Vol XL, págs. 855-864 (artículo completo)
F.A. Avid, L.C. Bessone, P. Gamazo, J.J. Penco, M.A. Pucheta, M.A. Storti (Eds.)
Concordia, 6-9 Noviembre 2023

FAILURE LOCALIZATION ANALYSIS OF CONCRETE SUBJECT TO HIGH TEMPERATURES

Sonia Vrech[a,c], Marianela Ripani[b,c], Paula Folino[b] and Guillermo Etse[a,b]

[a]*CEMNCI, Faculty of Exact Sciences and Engineering, National University of Tucuman, Argentina, svrech@herrera.unt.edu.ar, getse@herrera.unt.edu.ar*

[b]*LMNI, Faculty of Engineering, University of Buenos Aires, UBA-CONICET, Argentina, mripani@fi.uba.ar, pfolino@fi.uba.ar*

[c]*National Scientific and Technical Research Council (CONICET), Argentina*

Keywords: Failure analysis, Discontinuous bifurcation, Microplanes, High temperatures, Concrete.

Abstract. Despite the low thermal conductivity that characterizes concrete behavior, high temperatures acting for long periods on reinforced concrete structures could conduce to devastating effects on its overall integrity and stability. The caused damages comprises not only the structural, but also the material level, manifested as a degradation of the strength and stiffness properties, together with the increase of the porosity and the consequent loss of cohesion. In this work, the influence of high temperatures on the mechanical behavior of concrete is computationally evaluated by means of failure analysis in the form of discontinuous bifurcation. For this purpose, numerical solutions for the acoustic tensor for microplane-based plasticity theory are implemented. The nullity and/or negativity of the acoustic tensor suggests the potential development of localized failure, also allowing to know its orientation for a given stress state, concrete quality and applied high temperature.

1 INTRODUCTION

When quasi brittle materials like concrete are subjected to high temperatures in long term exposures, severe degradations in the mechanical properties (cohesion, friction, strength and stiffness) and changes in their failure mechanisms are evidenced as well as those caused by the action of loads or displacements. As a result of the dehydration process of the cement paste, there is an irreversible degradation of two fundamental material properties: the elastic stiffness (thermal damage) and the material strength (thermal decohesion). On the other hand, a particular failure or fracture mode develops, the so-called concrete spalling, characterized by superficial fracture planes parallel to the heated surface. Thermodynamically consistent constitutive models for quasi brittle materials subjected to long term exposures of elevated temperatures and for all possible stress path have been developed by the authors (Etse et al., 2016; Ripani et al., 2018; Vrech et al., 2021).

In the framework of the Smeared Crack Approach, localized failure modes are related to discontinuous bifurcations of the equilibrium path and lead to loss of ellipticity of the equations that govern the static equilibrium problem. The inhomogeneous or localized deformation field exhibits a plane of discontinuity that can be identified by means of the eigenvalue problem of the acoustic or localization tensor (Ottosen and Runesson, 1991). Analytical solutions for the discontinuous bifurcation condition, based on original works by Hadamard (1903); Thomas (1961); Hill (1962) conduce to the macroscopic localization condition. In this work the critical conditions for localized failure in the form of discontinuous bifurcation are analysed in the framework of the Microplane Theory, as proposed by Kuhl and Ramm (2000).

The microplane approach originally proposed by Bažant and Oh (1983) consists in the formulation of constitutive laws at microplane level defining the mechanical behavior of orientated planes. Then, the macroscopic response shall be achieved through the consideration of appropriated thermodynamically consistent homogenization process over the responses in all microplanes (Carol et al., 2001; Kuhl et al., 2001). The Microplanes Theory seems to be adequate to predict numerical and macroscopically the failure behavior of these materials, with the advantage of incorporating microstructure information. On the other hand, thermodynamically consistent theories are required to accurately simulate the complex behavior of quasi brittle materials. During the last decades, it has largely been used for predicting the mechanical behavior of quasibrittle materials such as concrete or rocks. Regarding cementitiuos materials, microplane based constitutive models have been approached by Huang et al. (2017); Indriyantho et al. (2020); Kong et al. (2023) a. o., whereas elasto-plastic microplane formulation for fiber reinforced concrete have been developed by Ferhun et al. (2013); Vrech et al. (2016); Xue and Kirane (2022).

In this work, the numerical analysis of the failure condition in microplane-based elasto-plasticity is evaluated for variable load states and temperature levels. Main purpose of this analysis is, on one hand, to evaluate the effect of temperature levels on the performance of the localization indicator or on the potential for localized failure. On the other hand, this analysis allows to evaluate the sensitivity of the orientation of temperature flux on the critical condition for discontinuous bifurcation.

After this introduction, Section 2 summarizes the thermodynamically consistent Microplane Theory. Then, Section 3 described the applied failure criterion, plastic potential and loading surfaces and Section 4, the temperature dependent elastic properties. Section 5 presents the analytical solution for localized failure in Microplane-based Elasto-Plasticity. Finally, Section 6 covers the numerical analysis of localization conditions.

2 THERMODYNAMICALLY CONSISTENT MICROPLANE THEORY

Regarding kinematic assumptions, thermodynamically consistent Microplane Theory is based on the projection of the macroscopic strain tensor $\boldsymbol{\varepsilon}$ on microplanes of normal direction $\boldsymbol{n}$. Normal and tangential strains at microplane level are computed by means the following relationships

$$\varepsilon_N = \boldsymbol{N} : \boldsymbol{\varepsilon} \quad , \quad \boldsymbol{\varepsilon}_T = \boldsymbol{T} : \boldsymbol{\varepsilon} \, , \tag{1}$$

with the projection tensors are defined as

$$\boldsymbol{N} = \boldsymbol{n} \otimes \boldsymbol{n} \quad , \quad \boldsymbol{T} = \boldsymbol{n} \cdot I^{sym} - \boldsymbol{n} \otimes \boldsymbol{n} \otimes \boldsymbol{n} \, , \tag{2}$$

being I^{sym} the symmetric part of the fourth-order identity tensor.

Assuming small strains in elasto-plastic regime, both macro- and microscopic strains are computed according to the Prandtl–Reuss additive decomposition. Particularly, at microplane level, normal and tangential strain rates are obtained as

$$\dot{\varepsilon}_N = \dot{\varepsilon}^e_N + \dot{\varepsilon}^p_N \quad , \quad \dot{\boldsymbol{\varepsilon}}_T = \dot{\boldsymbol{\varepsilon}}^e_T + \dot{\boldsymbol{\varepsilon}}^p_T \tag{3}$$

where the supra-indexes e and p denote elastic and plastic components, respectively.

The constitutive micro-stresses are derived from the free-energy potential at microplane level $\Psi = \Psi(\varepsilon^e_N, \boldsymbol{\varepsilon}^e_T, \kappa)$, being κ the scalar internal variable in case of isotropic hardening/softening. They are computed as

$$\sigma_N = \frac{\partial \psi^{mic}}{\partial \varepsilon_N} \quad , \quad \boldsymbol{\sigma}_T = \frac{\partial \psi^{mic}}{\partial \boldsymbol{\varepsilon}_{\boldsymbol{T}}} \quad , \quad \phi^{mic} = \frac{\partial \psi^{mic}}{\partial \kappa} \, , \tag{4}$$

being ϕ^{mic} the dissipative stress.

Assuming the macro free-energy potential as the integral of the micro free-energy on a spherical region of unit volume Ω, the following micro-macro free-energy relationship is established

$$\psi^{mac} = \frac{3}{4\pi} \int_{\Omega} \psi^{mic} \mathrm{d}\Omega \tag{5}$$

The evolution law of the free-energy potential at microplane level, regarding the kinematic projection of Eq. 1 is given by

$$\dot{\psi}^{mic} = \left(\boldsymbol{N} \sigma_N + \boldsymbol{T}^T \cdot \boldsymbol{\sigma}_T \right) : \dot{\boldsymbol{\varepsilon}}^{mac} + \phi^{mic} \dot{\kappa} \tag{6}$$

According to the Clausius–Duhem inequality, the homogenization of the microplanes energy leads to the definition of the macroscopic stress tensor in terms of the microscopic stress components

$$\boldsymbol{\sigma} = \frac{\partial \psi^{mac}}{\partial \boldsymbol{\varepsilon}} = \frac{3}{4\pi} \int_{\Omega} \boldsymbol{N} \sigma_N + \boldsymbol{T}^T \cdot \boldsymbol{\sigma}_T d\Omega \, . \tag{7}$$

This equation is solved through the by numerical integration techniques regarding all possible spatial directions by a weighted sum over a finite number of microplanes, as proposed by Bažant and Oh (1985)

$$\boldsymbol{\sigma} \approx \sum\nolimits_{I=1}^{n_{mp}} \left[\boldsymbol{N}^I {\sigma_N}^I + \boldsymbol{T}^{T,I} \cdot \boldsymbol{\sigma}^I_T \right] \mathrm{w}^I \tag{8}$$

being n_{mp} the adopted number of microplanes and w^I the corresponding weight coefficients.

3 MICROPLANE MODEL FOR CONCRETE UNDER HIGH TEMPERATURE

The temperature-dependent Microplane constitutive model is proposed by Vrech et al. (2021) based on the Microplane Theory consists on a the parabolic failure criterion in terms of the normal and tangential microstresses σ_N and $\boldsymbol{\sigma}_T$, respectively, as

$$\Phi = \alpha(T) \left[\frac{3(f_c' + f_t')^2}{8 f_t' f_c'^2} \right] \|\boldsymbol{\sigma}_T\|^2 + \sigma_N - \beta(T) f_t' = 0 \tag{9}$$

with f_t' and f_c', the uniaxial tensile and compressive strengths, respectively, and T the absolute temperature value that strongly degrades the comparison stress f_t'. $\alpha(T)$ and $\beta(T)$ are the temperature-dependent functions computed according to

$$\alpha(T) = 1 + \gamma_1 \, (T - 20) \ , \tag{10}$$

$$\beta(T) = 1 - \gamma_2 \, (T - 20) \ , \tag{11}$$

being γ_1 and γ_2 temperature-dependent values.

In the post-peak regime, the yield criterion softens according to

$$\Phi_s = \alpha(T) \left[\frac{3(f_c' + f_t')^2}{8 f_t' f_c'^2} \right] \|\boldsymbol{\sigma}_T\|^2 + \sigma_N - \beta(T) \phi^{mic} = 0 \, , \tag{12}$$

with the temperature dependent plastic potential, computed as

$$\Phi^* = \alpha(T) \left[\frac{3(f_c' + f_t')^2}{8 f_t' f_c'^2} \right] \|\boldsymbol{\sigma}_T\|^2 + \eta_T \, \sigma_N - \beta(T) \phi^{mic} = 0 \, , \tag{13}$$

being η_T the volumetric non-associativity degree. As a consequence of the cohesion loss, the volumetric plastic dilatation decreases with temperature. To account for this effect, the non-associativity degree increases with increasing temperature. The variation of η_T with respect to temperatures varying from $T_0 = 20$ to $T_{max} = 700$°C, is approximated by the function

$$\eta_T = \eta_{20} - (\eta_{20} - \eta_{Tmin}) \sin \left[\frac{\pi}{2} \frac{(T - T_0)}{(T_{max} - T_0)} \right] \ , \tag{14}$$

where η_{20} represents the non-associativity degree at 20 °C, η_{min} its minimal value, see Fig. 1.

The softening dissipative stress ϕ^{mic} is expressed in terms of the internal state variable κ and T. The strength degradation during post-peak processes is controlled by ϕ^{mic}. Figure (2) represents the variation of the maximum failure curve with increasing temperatures, from 20 to 600°C, represented in the stress space of coordinates σ_N-σ_T.

The dissipative stress, based on the Fracture Energy Theory, is obtained by

$$\phi^{mic} = f_t' \, \exp \left(\frac{-5 h_T}{u_r \, G_I} \dot{\kappa} \right) \tag{15}$$

being G_I the fracture energy in mode I type of failure, u_r the maximum crack opening displacement and h_T the corresponding characteristic length, that depends on the absolute temperature T according to

$$h_T = h \exp \left[-0.00308 (T - 20) \right] \tag{16}$$

where h corresponds to the material characteristic length at 20°C. Analysing Eqs. (12) and (15), it should be noted that the comparison strength decreases due to both, mechanical and thermal effects in softening regime.

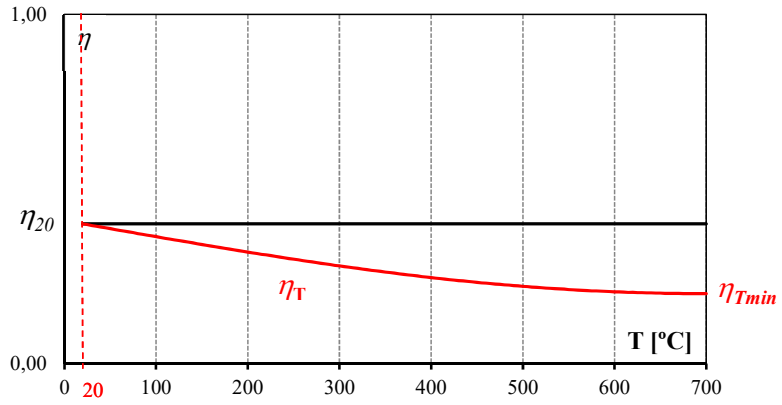

Figure 1: Variation of the volumetric non-associativity degree for variable temperature levels.

4 TEMPERATURE DEPENDENT ELASTIC PROPERTIES

As demostrated by Ripani et al. (2014), based in a large experimental database, the following expressions for the Young modulus E and Poisson coefficient ν for concrete can be applied to obtain the approximated values when the temperature level increases

$$E = E_0 \left(1 - \alpha_E T\right) \quad , \quad \nu = \nu_0 \left(1 - \alpha_\nu T\right) \tag{17}$$

being E_0 and ν_0 the elasticity modulus and Poisson coefficient at 20°C, respectively. Whereas α_E= 0.0014 and α_ν= 0.0010 are degradation parameters to be experimentally calibrated.

5 SOLUTION FOR LOCALIZED FAILURE IN MICROPLANE-BASED ELASTO-PLATICITY

In the framework of the Smeared Crack Approach, localized failure modes are related to discontinuous bifurcations of the equilibrium path, and lead to loss of ellipticity of the equations that govern the static equilibrium problem. The inhomogeneous or localized deformation field exhibits a plane of discontinuity that can be identified by means of the eigenvalue problem of the acoustic or localization tensor (Ottosen and Runesson, 1991). Analytical solutions for the discontinuous bifurcation condition, based on original works by Hadamard (1903); Thomas (1961); Hill (1962) conduce to the macroscopic localization condition

$$det(\boldsymbol{Q}^{ep}) = 0 \tag{18}$$

being $\boldsymbol{Q}^{ep}$ the elasto-plastic localization tensor, define as

$$\boldsymbol{Q}^{ep} = \boldsymbol{N} \cdot \boldsymbol{E}^{ep} \cdot \boldsymbol{N} \tag{19}$$

with $\boldsymbol{N}$, the normal direction to the discontinuity surface, see Fig. 3. According to Kuhl and Ramm (2000), in case of microplane-based plasticity the macroscopic elasto-plastic tangent operator can be obtained analogously to the macroscopic stresses in Eq. (8), as

$$\boldsymbol{E}^{ep} = \frac{d\boldsymbol{\sigma}}{d\boldsymbol{\varepsilon}} \approx \frac{3}{4\pi} \sum_{\Omega} \left[\boldsymbol{N} \otimes \frac{d\sigma_N}{d\varepsilon_N} + \boldsymbol{T}^T \cdot \frac{d\boldsymbol{\sigma}_T}{d\boldsymbol{\varepsilon}_T} \right] d\Omega \,. \tag{20}$$

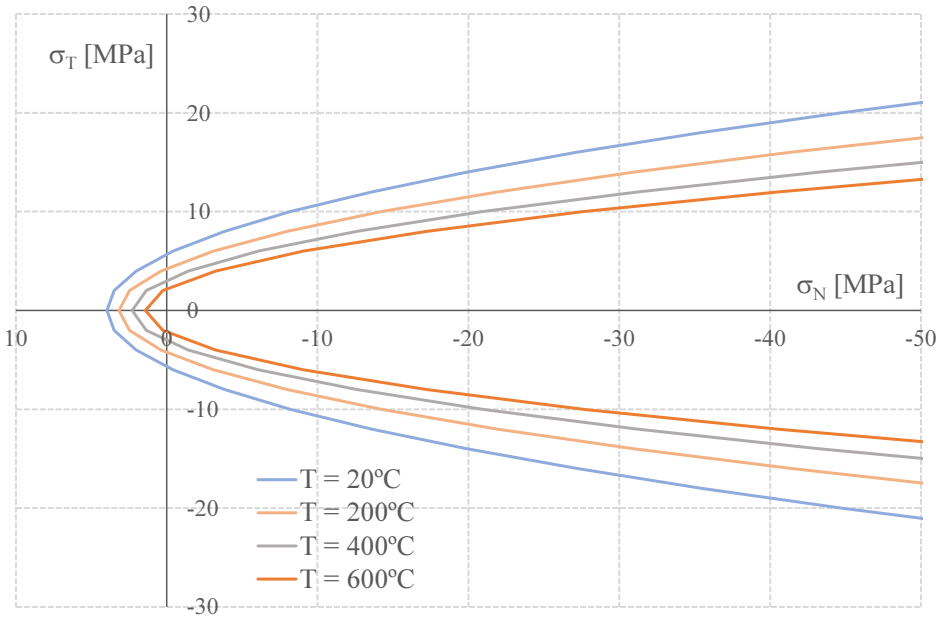

Figure 2: Microplane failure criterion degradation with increasing temperature.

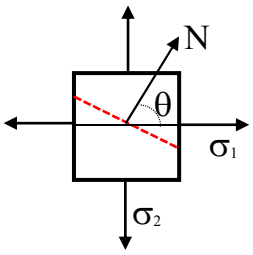

Figure 3: Numerical localization analysis at peak of the uniaxial tensile test.

Regarding the microplane constitutive formulation in Section 2, the above equation can be expressed as

$$\boldsymbol{E}^{ep} = \boldsymbol{E}^{e} - \frac{3}{4\pi}\sum_{\Omega}\frac{1}{h}\left[E_N\mu_N\boldsymbol{N} + E_T\boldsymbol{T}^T\cdot\boldsymbol{\mu}_T\right]\otimes\left[E_N\nu_N\boldsymbol{N} + E_T\boldsymbol{\nu}_T\cdot\boldsymbol{T}^T\right]d\Omega\,, \tag{21}$$

being

$$h = E_N\nu_N\mu_N + E_T\boldsymbol{\nu}_T\cdot\boldsymbol{\mu}_T + H\,, \tag{22}$$

with the isotropic hardening/softening modulus H and

$$\nu_N = \frac{\partial\Phi}{\partial\sigma_N}\quad,\quad \mu_N = \frac{\partial\Phi^*}{\partial\sigma_N}\quad,\quad \boldsymbol{\nu}_T = \frac{\partial\Phi}{\partial\boldsymbol{\sigma}_N}\quad,\quad \boldsymbol{\mu}_T = \frac{\partial\Phi^*}{\partial\boldsymbol{\sigma}_T}\,. \tag{23}$$

The elastic macroscopic tangent operator is given by

$$\boldsymbol{E}^{e} = \frac{3}{4\pi}\sum_{\Omega}E_N\boldsymbol{N}\otimes\boldsymbol{N} + E_T\boldsymbol{T}^T\cdot\boldsymbol{T}d\Omega\,. \tag{24}$$

Then, the elasto-plastic localization tensor in Eq. (18), results

$$\boldsymbol{Q}^{ep} \approx \boldsymbol{Q}^{e} - \frac{3}{4\pi}\sum_{\Omega}\frac{\boldsymbol{a}^*\otimes\boldsymbol{a}}{h}d\Omega\,. \tag{25}$$

with the elastic localization tensor $\boldsymbol{Q}^e = \boldsymbol{N} \cdot \boldsymbol{E}^e \cdot \boldsymbol{N}$ and the traction vectors computed as

$$\begin{aligned} \boldsymbol{a} &= [\nu_N E_N \boldsymbol{N} + E_T \boldsymbol{\nu}_T \cdot \boldsymbol{T}] \cdot \boldsymbol{N} \,, \\ \boldsymbol{a}^* &= \boldsymbol{N} \cdot \left[E_N \mu_N \boldsymbol{N} + E_T \boldsymbol{T}^T \cdot \boldsymbol{\mu}_T\right] \,. \end{aligned} \tag{26}$$

Due to the complex structure of the acoustic tensor for microplane-based plasticity, the analytical assessment is not easy. Instead, numerical solutions must be applied and Eq. (25) can be rewritten as

$$\boldsymbol{Q}^{ep} \approx \boldsymbol{Q}^e - \sum_{I=1}^{n_{mp}} \left[\frac{\boldsymbol{a}^{*I} \otimes \boldsymbol{a}^I}{h^I}\right] \mathrm{w}^I \,. \tag{27}$$

6 NUMERICAL SOLUTIONS FOR LOCALIZED FAILURE IN MICROPLANE-BASED ELASTO-PLATICITY

In this section, the performance of the discontinuous bifurcation condition in the form of localized failure given in Eq. (18), is evaluated for concrete under different temperature conditions. In this analysis, encompassing uniaxial tension, pure shear and biaxial compression states under plane stresses with variable temperatures between 20 and 700°C, are taking into account. Concrete material properties and internal parameters indicated in Table 1 are assumed.

Elastic modulus-E	19305.3 MPa
Poisson's ratio	ν= 0.2
Compressive strength-$f_c^{'}$	22.0 MPa
Tensile strength-$f_t^{'}$	2.7 MPa
Temperature-dependent values-$\gamma_1; \gamma_2$	0.00126; 0.00056 °C^{-1}
Non-associative degree at 20°C-η_{20}	0.5

Table 1: Material properties and internal parameters adopted for the numerical analysis.

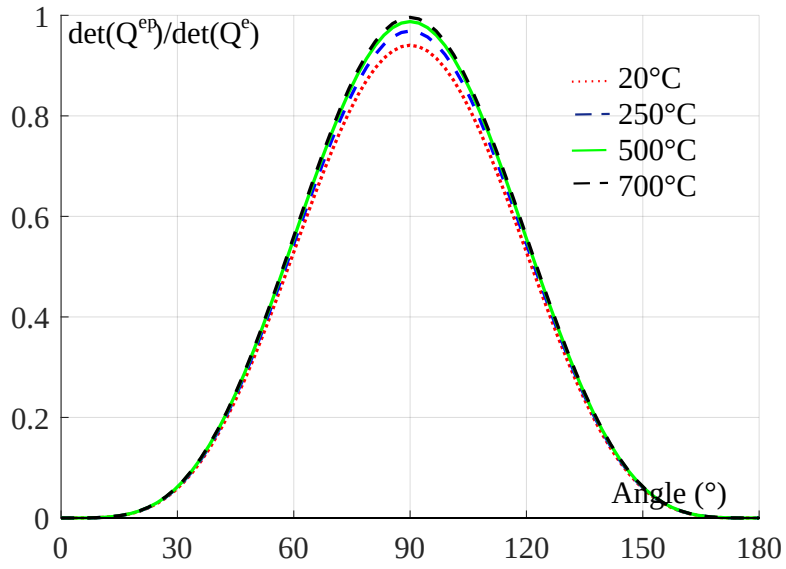

Figure 4: Numerical localization analysis at peak of the uniaxial tensile test.

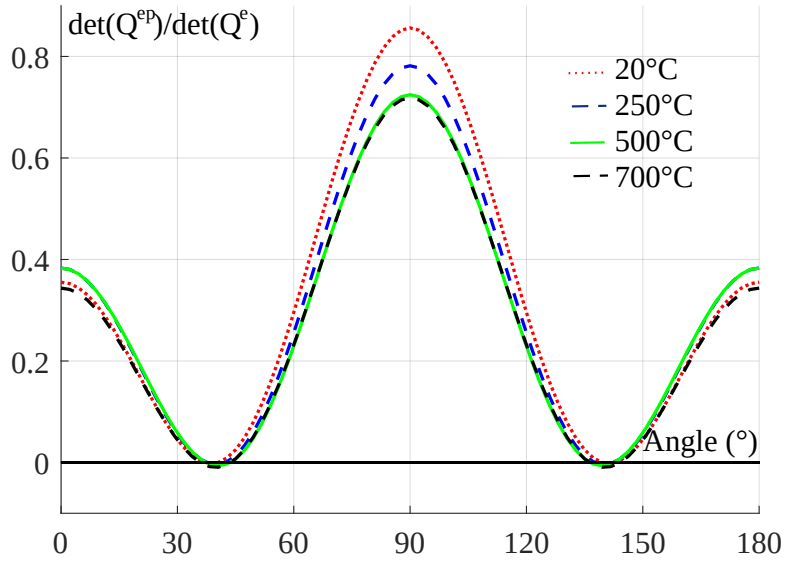

Figure 5: Numerical localization analysis at peak of the pure shear test.

Temperature (°C)	Critical localization angles (°)		
	Uniaxial tension	Pure shear	Biaxial compression
20	0-180	38.5-141.5	63.00-117.00
250	0-180	40.5-139.5	65.25-114.75
500	0-180	40.5-139.5	67.50-112.5
700	0-180	40.5-139.5	69.75-110.25

Table 2: Critical localization directions for uniaxial tension, pure shear and biaxial compression tests at different temperature levels.

In Figs. 4 to 6 the variation of the critical directions satisfying the localization condition are evaluated for variable temperature levels: T= 20, 250, 500 and 700°C, while the resulting critical localization directions are shown in Table 2.

Figure 4 shows the performance of the normalized localization condition $det(Q^{ep})/det(Q^{e})$ at peak of the uniaxial tensile test. The results demonstrate that the proposed Microplane constitutive Theory is able to capture that the localization condition is fulfilled for all temperatures at 0 and 180°.

Brittle or localized failure modes are also exhibited in the pure shear test and the biaxial compression tests (for all possible temperatures). Critical directions in case of pure shear tests are shown in Fig. 5. The critical directions results 38.5 and 141.5° for T= 20°C and 40.5-139.5° for the others. This increase in the value of the angles had also been captured by Ripani et al. (2018).

Whereas for biaxial tests, the obtained critical directions are 63.00-117.00°, 65.25-114.75°, 67.50-112.5° and 69.75-110.25° for increasing temperatures of 20, 250, 500 and 700°C, respectively, see Fig. 6.

The numerical solutions for discontinuous bifurcation of temperature dependent media in this work offer great potentials for more accurate predictions and understanding of concrete failure modes under different thermomechanical scenarios, and of their sensitivity to temperature.

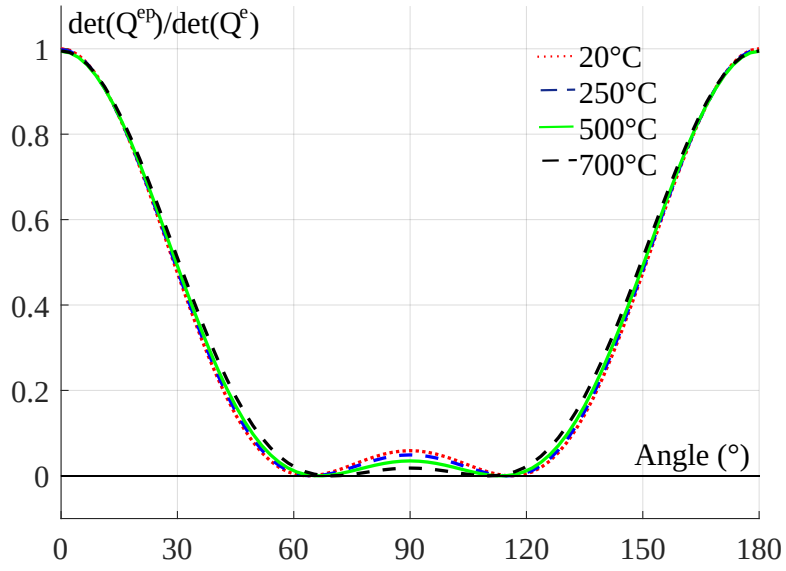

Figure 6: Numerical localization analysis at peak of the biaxial compression test.

7 CONCLUSIONS

In this work, a thermodynamically consistent Microplane Theory for quasi brittle materials like concrete, able to predict their failure behavior under high temperatures fields, has been presented.

The influence of high temperatures on the mechanical behavior of concrete is computationally evaluated by means of failure analysis in the form of discontinuous bifurcation. Analytical solutions for Microplane-based plasticity Theory have been developed, whereas numerical solutions for the acoustic tensor have been implemented to know critical directions with increasing temperatures at peak of the uniaxial tensile, pure shear and biaxial compression tests. The nullity and/or negativity of the acoustic tensor suggests the potential development of localized failure, also allowing to know its orientation for a given stress state, concrete quality and applied high temperature. Brittle or localized failure modes are exhibited for all possible temperatures in plane stress states.

ACKNOWLEDGEMENTS

The authors acknowledges the financial support for this work by SCAIT-UNT (Secretary of science, art and technological innovation of the University of Tucuman, Argentina) through the Grant PIUNT No. E754 and by University of Buenos Aires through the Grant UBACyT 2020 No. 20020190200208BA.

REFERENCES

Bažant Z. and Oh B. Crack band theory for fracture of concrete. *RILEM - Material Structures*, 93:155–177, 1983.

Bažant Z. and Oh B. Microplane model for progressive fracture of concrete and rock. *Journal of Engineering Mechanics*, 114(4):559–582, 1985.

Carol I., Jirasek M., and Bažant Z. A thermodynamically consistent approach to microplane theory. Part I. Free energy and consistent microplane stresses. *Int. J. of Solids and Structures*,

38(17):2921–2931, 2001.

Etse G., Vrech S., and Ripani M. Constitutive theory for recycled aggregate concretes subjected to high temperature. *Int. Journal of Construction and Building Materials*, 111:43–53, 2016.

Ferhun C., Caner F., Bažant Z., and Wendner R. Microplane model M7f for fiber reinforced concrete. *Engineering Fracture Mechanics*, 105:41–57, 2013.

Hadamard J. *Propagation des ondes et les equations d'Hydrodynamique*. Chelsea, New York, 1903.

Hager I. Behaviour of cement concrete at high temperature. *Bull. Pol. Acad. Sci. Tech. Sci.*, 61(1):2223–2241, 2013.

Hill R. Acceleration waves in solids. *J. Mech. Phys. Solids*, page 1–16, 1962.

Huang L., Li J., Tue N., and T. P. Numerical aspects of microplane constitutive models for concrete. *Applied Mathematical Modelling*, 38(41):530–548, 2017.

Indriyantho B., Zreid I., and Kaliske M. A nonlocal softening plasticity based on microplane theory for concrete at finite strains. *Computers and Structures*, 241:106333, 2020.

Kalifa P., Menneteau F., and Quenard D. Spalling and pore pressure in hpc at high temperatures. *Cem. Concr. Res.*, 30:1915–1927, 2000.

Kong L., Xie H., and Li C. Coupled microplane and micromechanics model for describing the damage and plasticity evolution of quasi-brittle material. *International Journal of Plasticity*, 162:103549, 2023.

Kuhl E. and Ramm E. Microplane modelling of cohesive frictional materials. *Eur. J. Mech.-A/Solids*, 19:121–143, 2000.

Kuhl E., Steinmann P., and Carol I. A thermodynamically consistent approach to microplane theory. Part II. Dissipation and inelastic constitutive modeling. *Int. J. of Solids and Structures*, 38(17):2933–2952, 2001.

Mindeguia J., Pimienta P., Noumowé A., and Kanema M. Temperature, pore pressure and mass variation of concrete subjected to high temperature: experimental and numerical discussion on spalling risk. *Cem. Concr. Res.*, 40:477–487, 2010.

Ottosen S. and Runesson K. Properties of discontinuous bifurcation solutions in elasto-plasticity. *Int. J. Solids Struct.*, 27:401–421, 1991.

Ripani M., E. G., Vrech S., and J. M. Thermodynamic gradient-based poroplastic theory for concrete under high temperatures. *Journal of Plasticity*, 61:v, 2014.

Ripani M., Vrech S., and E. G. Numerical assessment of temperature effects on concrete failure behavior. *Int. Journal of Fracture*, 212:219–236, 2018.

Thomas T. *Plastic Flow and Fracture in Solids*. Academic Press, London, 1961.

Vrech S., Etse G., and Caggiano A. Thermodynamically consistent elasto-plastic microplane formulation for fiber reinforced concrete. *Int. J. of Solids and Structures*, 81:337–349, 2016.

Vrech S., Ripani M., Etse G., and Folino P. Thermodynamic-consistent microplane theory for quasi brittle materials at high temperatures. *Mecánica Computacional*, XXXVIII:1071–1079, 2021.

Xue J. and Kirane K. Cylindrical microplane model for compressive kink band failures and combined friction/inelasticity in fiber composites I: Formulation. *Composite Structures*, 289:11538, 2022.

Zhang H. and Davie C. A numerical investigation of the influence of pore pressures and thermally induced stresses for spalling of concrete exposed to elevated temperatures. *Fire Saf. J.*, 59:102–110, 2013.